Fundamental Limits of Quantized MIMO ISAC under Gaussian Signaling

Hossein Atrsaei*, Mireille Sarkiss†, Michèle Wigger§
*LTCI, Télécom Paris, Institut Polytechnique de Paris, Palaiseau, France
Email: hossein.atrsaei@ip-paris.fr
†SAMOVAR, Télécom SudParis, Institut Polytechnique de Paris, Palaiseau, France
Email: mireille.sarkiss@telecom-sudparis.eu
§Université Paris-Saclay, CNRS, CentraleSupélec, Laboratoire des Signaux et Systèmes, 91190 Gif-sur-Yvette, France
Email: michele.wigger@centralesupelec.fr

***Abstract*—We study a quantized multiple-input multiple-output (MIMO) integrated sensing and communication (ISAC) system in which the communication and sensing receivers each apply analog spatial combining followed by scalar subtractive dithered quantization. This quantization model leads to an additive effective-noise representation with non-Gaussian noise. We derive upper and lower bounds on the capacity of this channel. Numerical results show that these bounds are tight at low signal-to-noise ratios (SNR) and saturate at high SNR due to finite-resolution quantization. They also show that, despite the effective noise being non-Gaussian, independent and identically distributed (i.i.d.) isotropic Gaussian signaling achieves rates close to capacity. Focusing on i.i.d. Gaussian signaling, this paper also presents a closed-form expression for the linear minimum mean-squared error (LMMSE) achieved under a Kronecker sensing-channel model. Numerical results show that the LMMSE also saturates at high SNR, where the saturation level increases as the spatial combining ratio decreases, and for combining ratios below one, saturation occurs even without quantization.**

***Index Terms*—Integrated sensing and communication (ISAC), Multiple input multiple output (MIMO), dithered quantizer, analog-to-digital converter (ADC), Gaussian signaling.**

I. Introduction

This work studies information-theoretic limits of integrated sensing and communication (ISAC) systems and the tradeoffs between communication and sensing performance in these systems. Previous works have characterized fundamental performance limits of ISAC systems under different channel models and sensing metrics [1]–[5].

A key practical limitation in large-scale multiple-input multiple-output (MIMO) systems is the power consumption and hardware cost of analog-to-digital converters (ADCs). Low-resolution ADCs, often combined with analog spatial processing prior to quantization, offer an effective way to reduce receiver complexity. The impact of coarse quantization on MIMO communication has been widely studied, including one-bit and low-resolution receiver architectures [6]–[10]. However, the capacity of quantized MIMO channels generally does not admit a closed-form expression, and existing works typically provide bounds or approximations for specific settings, such as one-bit ADCs or asymptotic regimes.

In this paper, we derive upper and lower bounds on the capacity of a MIMO ISAC system with spatial combiners and quantizers at the receiver side. The focus is on dithered quantization, which admits an additive-noise representation [11], but with a non-Gaussian noise. We assume channel state information at the communication receiver (CSIR) and no channel state information at the transmitter (no-CSIT). Our capacity lower bound follows from the worst-case noise property of Gaussian noise, while the upper bound follows from the maximum-entropy property of Gaussian random vectors. Numerical results show that our bounds are tight at low signal-to-noise ratios (SNR) and saturate at high SNR because of the limitations of the quantizers. Moreover, for all SNRs independent and identically distributed (i.i.d.) isotropic Gaussian signaling achieves rates close to capacity, despite the fact that quantization induces non-Gaussian noise.

We indeed consider a bi-static ISAC system in which the sensing receiver also processes its received signal through linear combiners and quantizers, before estimating the target response. For simplicity, a Kronecker model is used for the sensing channel [12]. In the spirit of *communication-centric* ISAC systems, we present a closed-form expression for the LMMSE at the sensing receiver under i.i.d. Gaussian signaling. Numerical results for Jakes channel model illustrate that the sensing LMMSE saturates at high SNR due to the quantization noise. They also show that, when spatial dimension reduction is applied (i.e, when the linear combiners map to smaller dimensions), saturation can occur even without quantization.

Notations: Random scalars, vectors, matrices, and sets are denoted by a, $\mathbf{\mathsf{a}}$, $\mathbf{\mathsf{A}}$, and A, respectively, while deterministic quantities are denoted by a, $\mathbf{a}$, $\mathbf{A}$, and $\mathcal{A}$. We denote the covariance matrix of a random vector $\mathbf{\mathsf{a}}$ by $\mathbf{R}_{\mathbf{\mathsf{a}}}$, and the Kronecker product and column-wise vectorization operators by $\otimes$ and $\mathrm{vec}(\cdot)$, respectively.

II. Channel Model and Performance Metrics

A. Channel Model

We consider the quantized MIMO ISAC architecture shown in Fig. 2. A transmitter equipped with N_t antennas sends a dual-functional random waveform $\mathbf{\mathsf{X}} = [\mathbf{\mathsf{x}}_1, \ldots, \mathbf{\mathsf{x}}_T] \in \mathbb{C}^{N_t \times T}$ over a coherence block of $T \geq N_t$ channel uses, serving simultaneously for communication and sensing. The transmit

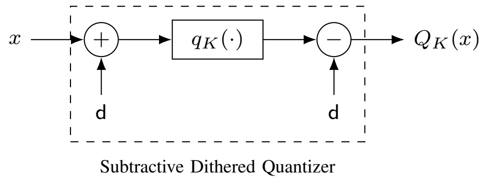

Fig. 1. Subtractive dithered quantizer.

covariance matrix is $\mathbf{R}_{\mathsf{X}} = \mathbb{E}\left[\frac{1}{T}\mathsf{X}\mathsf{X}^H\right]$ with the average power constraint $\mathrm{Tr}(\mathbf{R}_{\mathsf{X}}) = N_t P_0$.

The unquantized received signals at the communication and sensing receivers are

$$\mathsf{Y}_c = \mathsf{H}\mathsf{X} + \mathsf{W}_c, \tag{1a}$$

$$\mathsf{Y}_s = \mathsf{G}\mathsf{X} + \mathsf{W}_s. \tag{1b}$$

Here, $\mathsf{H} \in \mathbb{C}^{N_c \times N_t}$ denotes the communication channel, and $\mathsf{G} \in \mathbb{C}^{N_s \times N_t}$ denotes the sensing (target-response) channel. The noise matrices have independent circularly symmetric complex Gaussian (CSCG) entries across antennas and channel uses, with $\mathsf{w}_c \triangleq \mathrm{vec}(\mathsf{W}_c) \sim \mathcal{CN}(\mathbf{0}, \sigma_c^2 \mathbf{I}_{N_c T})$ and $\mathsf{w}_s \triangleq \mathrm{vec}(\mathsf{W}_s) \sim \mathcal{CN}(\mathbf{0}, \sigma_s^2 \mathbf{I}_{N_s T})$. The communication channel has i.i.d. Rayleigh-fading entries, i.e., $\mathrm{vec}(\mathsf{H}) \sim \mathcal{CN}(\mathbf{0}, \mathbf{I}_{N_t N_c})$.

The sensing channel follows the Kronecker correlation model [12]

$$\mathsf{G} = \mathbf{R}_A^{1/2} \mathsf{G}_0 \big(\mathbf{R}_B^{1/2}\big)^T, \qquad \mathbf{R}_{\mathsf{g}} = \mathbf{R}_B \otimes \mathbf{R}_A, \tag{2}$$

where $\mathsf{g} \triangleq \mathrm{vec}(\mathsf{G})$, G_0 has i.i.d. $\mathcal{CN}(0,1)$ entries, $\mathbf{R}_B \in \mathbb{C}^{N_t \times N_t}$ is the transmit-side correlation matrix, and $\mathbf{R}_A \in \mathbb{C}^{N_s \times N_s}$ is the receive-side correlation matrix. The sensing receiver is assumed to know the transmitted waveform X, as in the MIMO ISAC model of [13]. The transmitter has no channel state information about H, so the input distribution p_{X} cannot depend on the realization of H.

Each receiver adopts the hardware-limited quantization architecture of [14]–[16], consisting of an analog spatial combiner followed by parallel scalar ADCs. For each snapshot $t \in \{1, \ldots, T\}$ and each receiver $r \in \{c, s\}$, the received vector $\mathsf{y}_{r,t} \in \mathbb{C}^{N_r}$ is processed by a deterministic analog combiner $\mathbf{A}_r \in \mathbb{C}^{\tilde{N}_r \times N_r}$ as

$$\mathsf{u}_{r,t} = \mathbf{A}_r \mathsf{y}_{r,t}, \qquad r \in \{c, s\}, \quad t = 1, \ldots, T. \tag{3}$$

The combiner is constrained to be semi-unitary,

$$\mathbf{A}_r \mathbf{A}_r^H = \mathbf{I}_{\tilde{N}_r}, \qquad r \in \{c, s\}, \tag{4}$$

which prevents noise amplification and preserves the spatial whiteness of the receiver noise after combining.

The real and imaginary parts of each entry of $\mathsf{u}_{r,t}$ are quantized independently using a K-level subtractive dithered uniform quantizer, shown in Fig. 1. For a real input x, the quantizer output is

$$Q_K(x) = q_K(x + \mathsf{d}) - \mathsf{d}, \tag{5}$$

where d is an independent dither uniformly distributed over $[-\Delta_r/2, \Delta_r/2]$. The map $q_K(\cdot)$ is a K-level uniform scalar quantizer with dynamic range $[-\gamma_r, \gamma_r]$ and step size $\Delta_r = 2\gamma_r/K$. The dynamic range is partitioned into K subintervals of width Δ_r, whose midpoints are the reconstruction levels. Inputs outside $[-\gamma_r, \gamma_r]$ are saturated to the nearest reconstruction level, namely $\pm(\gamma_r - \Delta_r/2)$.

Under Schuchman's conditions [17], [18], and assuming negligible overload, the subtractive dithered quantizer yields an additive-noise representation in which the quantization error is statistically independent of the input [11]. Thus, for each receiver $r \in \{c, s\}$ and snapshot t,

$$\mathsf{z}_{r,t} = \mathsf{u}_{r,t} + \mathsf{w}_{q,r,t}, \tag{6}$$

where the entries of $\mathsf{w}_{q,r,t}$ are independent, with independent real and imaginary parts uniformly distributed over $[-\Delta_r/2, \Delta_r/2]$. Consequently,

$$\mathbb{E}\big[|(\mathsf{w}_{q,r,t})_i|^2\big] = \frac{\Delta_r^2}{6}. \tag{7}$$

The dynamic range γ_r must be chosen large enough so that the dithered input remains within $[-\gamma_r, \gamma_r]$ with high probability. For notational compactness, we stack the samples over one coherence block as $\mathsf{u}_r = \mathrm{vec}\big([\mathsf{u}_{r,1}, \ldots, \mathsf{u}_{r,T}]\big)$, and define d_r, $\mathsf{w}_{q,r}$, z_r, and the other block-level vectors analogously. Following [14]–[16], we set

$$\gamma_r = \eta \sqrt{\max_{i=1,\ldots,\tilde{N}_r T} \mathbb{E}\Big[\big|(\mathsf{u}_r + \mathsf{d}_r)_i\big|^2\Big]}, \qquad r \in \{c, s\}, \tag{8}$$

where $\eta > 0$ controls the overload probability. Since

$$\mathbb{E}\Big[\big|(\mathsf{u}_r + \mathsf{d}_r)_i\big|^2\Big] = (\mathbf{R}_{\mathsf{u}_r})_{i,i} + \frac{\Delta_r^2}{6}, \tag{9}$$

and since $\Delta_r = 2\gamma_r/K$, we obtain

$$\gamma_r^2 = \kappa \max_{i=1,\ldots,\tilde{N}_r T} (\mathbf{R}_{\mathsf{u}_r})_{i,i}\,, \tag{10}$$

where

$$\kappa \triangleq \eta^2 \left(1 - \frac{2\eta^2}{3K^2}\right)^{-1}. \tag{11}$$

This expression is well defined when $\eta < \sqrt{3/2}\,K$.

The stacked pre-quantization and quantized signals are

$$\mathsf{u}_r = (\mathbf{I}_T \otimes \mathbf{A}_r)\mathsf{y}_r, \qquad \mathsf{z}_r = \mathsf{u}_r + \mathsf{w}_{q,r}, \tag{12}$$

where $\mathsf{y}_r \triangleq \mathrm{vec}(\mathsf{Y}_r)$. Substituting (1) into (12) gives the quantized sensing and communication models

$$\mathsf{z}_s = (\mathsf{X}^T \otimes \mathbf{A}_s)\mathsf{g} + \bar{\mathsf{w}}_s, \tag{13a}$$

$$\mathsf{z}_c = (\mathbf{I}_T \otimes \mathbf{A}_c \mathsf{H})\mathsf{x} + \bar{\mathsf{w}}_c, \tag{13b}$$

where $\mathsf{x} \triangleq \mathrm{vec}(\mathsf{X})$ and

$$\bar{\mathsf{w}}_r \triangleq (\mathbf{I}_T \otimes \mathbf{A}_r)\mathsf{w}_r + \mathsf{w}_{q,r}, \qquad r \in \{c, s\}, \tag{14}$$

is the effective noise vector. The noise components w_r and $\mathsf{w}_{q,r}$ are mutually independent and have i.i.d. entries with variances σ_r^2 and $\Delta_r^2/6 = 2\gamma_r^2/(3K^2)$, respectively. Combining these observations with (10) and the semi-unitary constraint (4), the effective noise covariance becomes

$$\mathbf{R}_{\bar{\mathsf{w}}_r} = \sigma_{0,r}^2 \mathbf{I}_{\tilde{N}_r T}, \qquad r \in \{c, s\}, \tag{15}$$

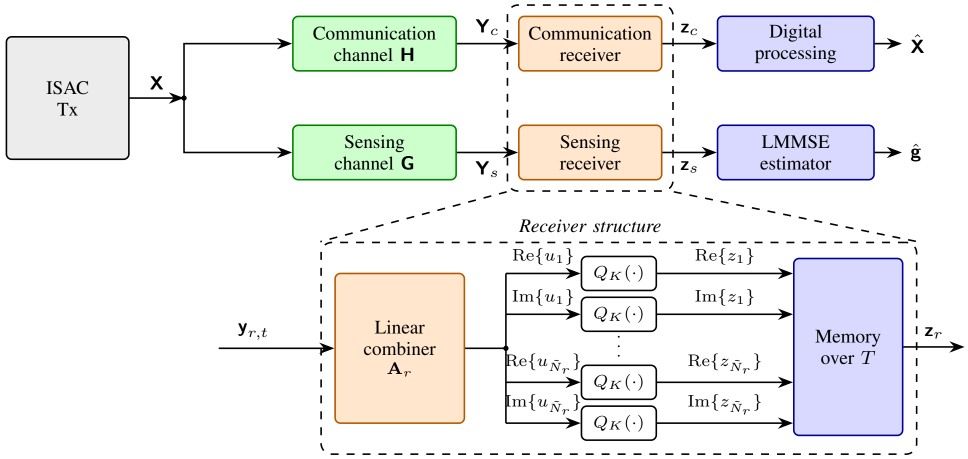

Fig. 2. Quantized MIMO-ISAC system model. The transmitted random waveform $\mathbf{X} \in \mathbb{C}^{N_t \times T}$ is observed as $\mathbf{Y}_c = \mathbf{H}\mathbf{X} + \mathbf{W}_c$ at the communication receiver and as $\mathbf{Y}_s = \mathbf{G}\mathbf{X} + \mathbf{W}_s$ at the sensing receiver. Both receivers employ the same quantization architecture of [14]–[16]: for each snapshot, the received vector $\mathbf{y}_{r,t}$ is linearly combined by $\mathbf{A}_r$, each real and imaginary component of the resulting complex entries is quantized by a scalar subtractive dithered quantizer $Q_K(\cdot)$, and the quantized outputs are accumulated in memory over the coherence block.

where, for each $r \in \{c, s\}$,

$$\sigma_{0,r}^2 \triangleq \sigma_r^2 + \beta \max_{i=1,\ldots,\tilde{N}_r T} (\mathbf{R}_{\mathbf{u}_r})_{i,i}\,, \qquad \beta \triangleq \frac{2\kappa}{3K^2}. \tag{16}$$

B. Performance Metrics

1) Sensing distortion: The sensing performance is measured by the normalized LMMSE in estimating the target-response vector $\mathbf{g}$. Since the sensing receiver knows the realization of the transmitted waveform $\mathbf{X} = \mathbf{X}$, the conditional sensing model is linear in $\mathbf{g}$. The LMMSE estimator is therefore [19]

$$\hat{\mathbf{g}} = \mathbf{R}_{\mathbf{g}} \tilde{\mathbf{X}}^H \left(\tilde{\mathbf{X}} \mathbf{R}_{\mathbf{g}} \tilde{\mathbf{X}}^H + \mathbf{R}_{\bar{\mathbf{w}}_s} \right)^{-1} \mathbf{z}_s, \tag{17}$$

where

$$\tilde{\mathbf{X}} \triangleq \mathbf{X}^T \otimes \mathbf{A}_s. \tag{18}$$

The corresponding LMMSE error covariance matrix is

$$\mathbf{R}_{\mathbf{g}|\mathbf{z}_s, \mathbf{X}=\mathbf{X}} = \mathbf{R}_{\mathbf{g}} - \mathbf{R}_{\mathbf{g}} \tilde{\mathbf{X}}^H \left(\tilde{\mathbf{X}} \mathbf{R}_{\mathbf{g}} \tilde{\mathbf{X}}^H + \mathbf{R}_{\bar{\mathbf{w}}_s} \right)^{-1} \tilde{\mathbf{X}} \mathbf{R}_{\mathbf{g}}. \tag{19}$$

The conditional LMMSE is given by the trace of (19), which by the Woodbury matrix identity simplifies to:

$$\sigma_{\mathbf{g}|\mathbf{X}=\mathbf{X}}^2(\mathbf{A}_s) = \frac{1}{N_t N_s} \mathrm{Tr}\left(\left[\mathbf{R}_{\mathbf{g}}^{-1} + \frac{1}{\sigma_{0,s}^2} \left(\mathbf{X}^* \mathbf{X}^T \otimes \mathbf{A}_s^H \mathbf{A}_s \right) \right]^{-1} \right). \tag{20}$$

For a given input distribution $p_{\mathbf{X}}$, the sensing distortion is obtained by minimizing the expected conditional LMMSE distortion over all admissible sensing combiners:

$$\epsilon(p_{\mathbf{X}}) \triangleq \min_{\mathbf{A}_s :\, \mathbf{A}_s \mathbf{A}_s^H = \mathbf{I}_{\tilde{N}_s}} \mathbb{E}_{\mathbf{X}} \left[\sigma_{\mathbf{g}|\mathbf{X}}^2(\mathbf{A}_s) \right]. \tag{21}$$

2) Communication rate: Since the communication receiver has perfect channel state information, for a given input distribution $p_{\mathbf{X}}$, the following rate is achievable:

$$R(p_{\mathbf{X}}) \triangleq \frac{1}{T} \max_{\mathbf{A}_c :\, \mathbf{A}_c \mathbf{A}_c^H = \mathbf{I}_{\tilde{N}_c}} I(\mathbf{X}; \mathbf{Z}_c \mid \mathbf{H}), \tag{22}$$

where $\mathbf{Z}_c \triangleq [\mathbf{z}_{c,1}, \ldots, \mathbf{z}_{c,T}]$.

III. Performance under Gaussian Signaling

We consider i.i.d. isotropic Gaussian signaling, i.e., the transmitted symbols are independent across time and

$$\mathbf{x}_t \sim \mathcal{CN}(\mathbf{0}, P_0 \mathbf{I}_{N_t}), \qquad t = 1, \ldots, T. \tag{23}$$

Thus, $\mathbf{R}_{\mathbf{X}} = P_0 \mathbf{I}_{N_t}$. For this input distribution, we denote the sensing distortion $\epsilon(p_{\mathbf{X}})$ and the communication rate $R(p_{\mathbf{X}})$ by ϵ_G and R_G, respectively. In the following, we characterize ϵ_G and provide bounds on R_G, which is difficult to characterize exactly due to the non-Gaussian effective noise.

A. Bounds on R_G

As shown in Appendix A-A, under isotropic Gaussian signaling, irrespective of the choice of the linear combiner and the channel $\mathbf{H}$,

$$\sigma_{0,c}^2 = \sigma_c^2 + \beta(\sigma_c^2 + N_t P_0). \tag{24}$$

Let $\lambda_1(\mathbf{H}\mathbf{H}^H) \geq \cdots \geq \lambda_{N_c}(\mathbf{H}\mathbf{H}^H)$ denote the ordered eigenvalues of $\mathbf{H}\mathbf{H}^H$, and define

$$R_{\mathrm{G,L}} \triangleq \mathbb{E}_{\mathbf{H}} \left[\sum_{i=1}^{\tilde{N}_c} \log \left(1 + \frac{P_0 \lambda_i(\mathbf{H}\mathbf{H}^H)}{\sigma_{0,c}^2} \right) \right], \tag{25}$$

and

$$R_{\mathrm{G,U}} \triangleq R_{\mathrm{G,L}} + \tilde{N}_c \log\left(\pi e \sigma_{0,c}^2 \right) - 2\tilde{N}_c\, h\left(\mathrm{Re}(\bar{\mathsf{W}}_{c,i}) \right), \tag{26}$$

where $\mathrm{Re}(\bar{\mathsf{W}}_c)$ denotes the real part of one scalar component of the effective communication noise. Its density is

$$f_{\mathrm{Re}(\bar{\mathsf{W}}_c)}(w) = \frac{1}{\Delta_c}\left[Q\left(\frac{w-\Delta_c/2}{\sigma_c/\sqrt{2}}\right) - Q\left(\frac{w+\Delta_c/2}{\sigma_c/\sqrt{2}}\right)\right], \tag{27}$$

with $Q(\cdot)$ denoting the standard Gaussian Q-function.

Notic that the lower bound R_{G} only captures the dominant $\tilde{N}_c$ eigenmodes of $(\mathbf{H}\mathbf{H}^H)$, but not the smaller eigenmodes.

Theorem 1 (Bounds on R_G)**.** *Under Gaussian signaling, the achievable rate satisfies*

$$R_{\mathrm{G,L}} \leq R_{\mathrm{G}} \leq R_{\mathrm{G,U}}. \tag{28}$$

Proof: See Appendix A. ∎

Remark 1. The upper bound in Theorem 1 is also an upper bound on capacity. As a consequence, when the two bounds coincide, isotropic Gaussian signaling is capacity-achieving. Our numerical results in Section IV show that this is indeed the case in the low and moderate SNR regimes.

The bounds in (28) admit simple interpretations in several asymptotic regimes. We express these regimes in terms of

$$\mathrm{SNR} \triangleq \frac{N_t P_0}{\sigma_c^2}. \tag{29}$$

Low SNR. For $P_0/\sigma_c^2 \to 0$, we have $\sigma_{0,c}^2 = \sigma_c^2(1+\beta)+o(1)$. Using $\log(1+x) = x + o(x)$ gives

$$R_{\mathrm{G,L}} = \frac{P_0}{\sigma_c^2(1+\beta)}\mathbb{E}_{\mathbf{H}}\left[\sum_{i=1}^{\tilde{N}_c}\lambda_i(\mathbf{H}\mathbf{H}^H)\right] + o(P_0). \tag{30}$$

Thus, quantization induces a multiplicative penalty $1+\beta$ on the low-SNR slope.

High SNR with fixed resolution. For $P_0/\sigma_c^2 \to \infty$ with fixed K, the effective-noise variance grows linearly with P_0:

$$\sigma_{0,c}^2 = \beta N_t P_0 + o(P_0). \tag{31}$$

Consequently, the lower bound saturates as

$$\lim_{P_0\to\infty} R_{\mathrm{G,L}} = \mathbb{E}_{\mathbf{H}}\left[\sum_{i=1}^{\tilde{N}_c}\log\left(1+\frac{\lambda_i(\mathbf{H}\mathbf{H}^H)}{\beta N_t}\right)\right]. \tag{32}$$

High resolution. As $\Delta_c \to 0$, the quantization noise vanishes and

$$h\big(\mathrm{Re}(\bar{\mathsf{W}}_c)\big) \to \frac{1}{2}\log\big(\pi e \sigma_c^2\big). \tag{33}$$

Therefore, the gap $R_{\mathrm{G,U}} - R_{\mathrm{G,L}}$ tends to zero, and the lower and upper bounds become asymptotically tight. In this regime, both bounds converge to the Gaussian MIMO capacity without quantization.

Massive MIMO. By the favorable-propagation and channel-hardening properties of i.i.d. Rayleigh massive MIMO channels [20], as $N_t/\tilde{N}_c \to \infty$,

$$R_{\mathrm{G,L}} \longrightarrow \tilde{N}_c \log\left(1+\frac{N_t P_0}{\sigma_{0,c}^2}\right). \tag{34}$$

B. Closed-Form Expression for ϵ_G

Adapting [14, Appendix A] to the present model, we obtain:

Theorem 2 (Closed-form expression for ϵ_G)**.** *Under i.i.d. isotropic Gaussian signaling, i.e., $\mathbf{R}_{\mathbf{X}}^* = P_0\mathbf{I}_{N_t}$,*[1]

$$\begin{aligned}\epsilon_G = &\frac{1}{N_t N_s}\mathrm{Tr}(\mathbf{R}_B \otimes \mathbf{R}_A)\\ &-\frac{1}{N_t N_s}\max_{\{\sigma_i^2\geq 0\}}\sum_{n=1}^{N_t}\sum_{i=1}^{\tilde{N}_s}\frac{\mathrm{Tr}(\mathbf{R}_B)}{N_t}\\ &\cdot\mathbb{E}_{\mathbf{X}}\left[\frac{\lambda_{A,i}\,\lambda'_n\,\sigma_i^2}{\lambda'_n\sigma_i^2 + \frac{\beta}{\tilde{N}_s}\mathrm{Tr}(\mathbf{R}_{\mathbf{X}}^*\mathbf{R}_B)\sum_{j=1}^{\tilde{N}_s}\sigma_j^2 + \sigma_s^2(1+\beta)}\right],\end{aligned} \tag{35}$$

where $\{\lambda_{A,i}\}$ and $\{\lambda'_n\}$ are the eigenvalues of $\mathbf{R}_A$ and $\mathbf{R}_B^{1/2}\mathbf{X}^*\mathbf{X}^T(\mathbf{R}_B^{1/2})^H$ in descending order, and maximization is subject to

$$\sum_{i=N_s-\tilde{N}_s+1}^{N_s}\lambda_{A,i} \;\leq\; \sum_{i=1}^{\tilde{N}_s}\sigma_i^2 \;\leq\; \sum_{i=1}^{\tilde{N}_s}\lambda_{A,i}. \tag{36}$$

Proof: See Appendix B. ∎

IV. Numerical Results

Unless stated otherwise, the transmitter has $N_t = 16$ antennas and each receiver has 16 antennas, i.e., $N_c = N_s = 16$. The coherence length is $T = 40$ channel uses, and the noise variances are $\sigma_c^2 = \sigma_s^2 = 10^{-3}$. The dither overload factor is set to $\eta = 1$.

We define the combining ratios as

$$r_r \triangleq \tilde{N}_r/N_r, \quad r \in \{c, s\}, \tag{37}$$

and use the SNR defined in (29); since $\sigma_c^2 = \sigma_s^2$ here, it coincides with $N_t P_0/\sigma_s^2$ for the sensing plots.

The sensing channel is modeled with Jakes correlations [21]

$$\begin{aligned}(\mathbf{R}_A)_{n_1,n_2} &= J_0(\pi|n_1-n_2|)\,,\\ (\mathbf{R}_B)_{n_1,n_2} &= J_0(0.8\pi|n_1-n_2|)\,,\end{aligned}$$

where $J_0(\cdot)$ is the zero-order Bessel function of the first kind.

Expectation over $\mathbf{H}$ in (25) is calculated using Monte Carlo method, and the entropy term $h(\mathrm{Re}(\bar{\mathsf{W}}_c))$ in (26) is computed by numerical integration of the density in (27).

Fig. 3 illustrates the bounds of Theorem 1 on the Gaussian-signaling rate R_G versus SNR, as well as the unquantized no-combiner reference $\mathbb{E}_{\mathbf{H}}\big[\sum_i \log\big(1+P_0\lambda_i(\mathbf{H}\mathbf{H}^H)/\sigma_c^2\big)\big]$, for combining ratio $r_c = 1$. For this value, the optimal combiner is the identity and the Gaussian rate R_{G} can be computed numerically. We observe that at low and moderate SNRs, the lower bound $R_{\mathrm{G,L}}$, the exact rate R_G, and the upper bound $R_{\mathrm{G,U}}$ are indistinguishably close. This holds because the Gaussian noise dominates the effective noise. Since $R_{\mathrm{G,U}}$ is also an upper bound on capacity, we can also deduce that i.i.d. isotropic Gaussian signaling operates close to capacity in

[1]The expression in (35) holds for any feasible input covariance $\mathbf{R}_{\mathbf{X}} \succeq \mathbf{0}$ satisfying $\mathrm{Tr}(\mathbf{R}_{\mathbf{X}}) = N_t P_0$.

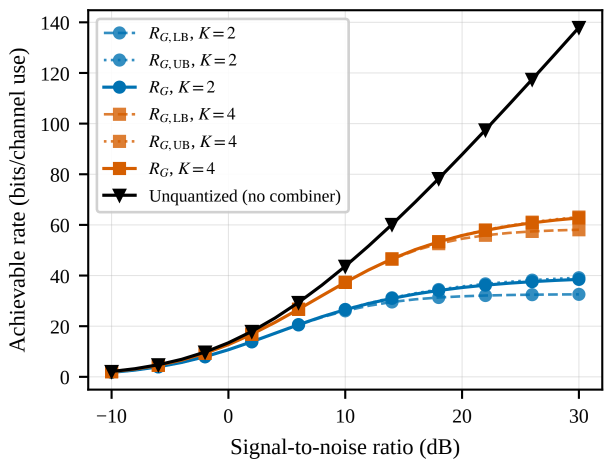

Fig. 3. Lower and upper bounds, exact rate, and unquantized no-combiner reference plotted versus SNR for ADC resolutions $K \in \{2, 4\}$ ($N_t = 16$, $r_c = 1$, and $T = 40$).

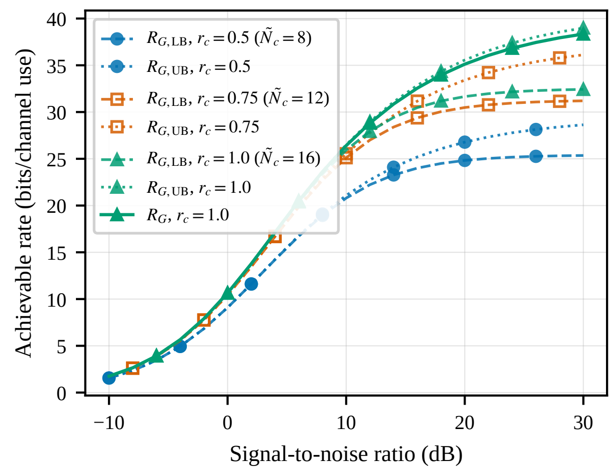

Fig. 4. Lower and upper bounds, exact rate (for $r_c = 1$), and unquantized no-combiner reference plotted versus SNR for combining ratios $r_c \in \{0.5, 0.75, 1\}$ ($N_t = 16$, $K = 2$, $T = 40$).

these regimes. At high SNR, a moderate gap appears between both bounds and the exact R_{G}, which is due to the non-Gaussianity of the effective noise induced by quantization. Both the Gaussian rate R_{G} and capacity saturate in the high SNR regime, because the quantization-noise variance increases with the transmit power. Finally, compared with the unquantized no-combiner benchmark, we deduce that at very low SNR, quantization induces only a negligible rate penalty, in particular if the quantizer resolution K is sufficiently large ($K = 4$).

Fig. 4 shows the effect of the communication combining ratio r_c on the rate, plotting the bounds of Theorem 1 versus SNR for $r_c \in \{0.5, 0.75, 1\}$ at fixed resolution $K = 2$. For $r_c = 0.5$ and $r_c = 0.75$, only a fraction of the 16 spatial dimensions are retained before quantization, whereas for $r_c = 1$ all dimensions are kept and the exact rate R_G can again be computed. At low SNR all combining ratios coincide, since in this regime the rate is noise-limited rather than dimension-limited. As the SNR increases, the impact of the combining ratio becomes more pronounced. The curves for $r_c = 0.75$ and $r_c = 1$ remain nearly indistinguishable up to the moderate-SNR regime, whereas the more substantial dimensionality reduction with $r_c = 0.5$ starts to show a visible rate loss earlier

Fig. 5 compares the Gaussian-signaling LMMSE ϵ_G with the unquantized distortion obtained with the optimal linear combiner under the Gaussian signaling. In the expression for ϵ_G in (35), the expectation has no closed form for a general $\mathbf{R}_B$. We therefore approximate it by sample-average approximation (SAA): we draw independent waveform samples according to (23), compute the eigenvalues of $\mathbf{R}_B^{1/2}\mathbf{X}^*\mathbf{X}^T(\mathbf{R}_B^{1/2})^H$ for each sample, and replace $\mathbb{E}_{\mathbf{X}}[\cdot]$ in (35) by the corresponding empirical average. The resulting finite-sample optimization over $\{\sigma_i\}_{i=1}^{\tilde{N}_s}$ is then solved numerically under (36).

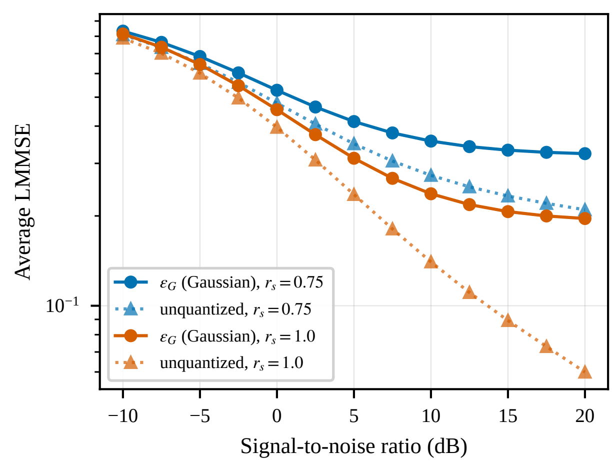

Fig. 5. Gaussian-signaling distortion ϵ_G versus SNR for the Jakes channel ($N_t = 16$, $K = 2$, $r_s \in \{0.75, 1\}$), with the unquantized reference.

From Fig. 5, we observe that ϵ_G saturates at high SNR. Thus, quantization induces saturation not only in the communication rate, but also in the sensing LMMSE. In contrast, the unquantized benchmark tends to zero when $r_s = 1$, since no spatial dimension is discarded. However, when $r_s = 0.75$, the unquantized benchmark also saturates because the linear combiner reduces the dimension of the sensing observations before estimation. In fact, the unquantized curve with $r_s = 0.75$ saturates at a higher LMMSE level than the quantized curve with $r_s = 1$. This indicates that, once dimension reduction is present, the dominant sensing loss may come from discarding spatial observations rather than from quantization itself.

V. Conclusion and Future Work

We studied a quantized MIMO ISAC system in which both the communication and sensing receivers employ analog spatial combining followed by scalar subtractive dithered quantization. Focusing on i.i.d. isotropic Gaussian signaling under no-CSIT and CSIR, we characterized the LMMSE sensing distortion using optimization and majorization tools, and derived information-theoretic lower and upper bounds on the corresponding achievable communication rate. The proposed upper bound is also an upper bound on capacity.

Numerical results suggest that the proposed lower and upper bounds on the Gaussian-input communication rate are tight at low and moderate SNRs, and thus Gaussian signaling is near-optimal. At high SNR, the achievable communication rates saturate at a level determined by the number of quantization levels K.

For sensing, we derived a closed-form expression for the LMMSE under i.i.d. Gaussian signaling and a Kronecker sensing-channel model. Numerical results show that the LMMSE saturates at high SNR, whereas at low SNR it remains close to the corresponding unquantized LMMSE with the same spatial combiner. The saturation level increases when the sensing combining ratio is reduced, and for combining ratios below one, saturation can occur even without quantization. This shows that both quantization and spatial dimension reduction can fundamentally limit the sensing accuracy, whereas dimension reduction has only a minor effect on the achievable rate.

Future work includes tightening the capacity bounds, particularly in the high-SNR regime; see also [11]. When no spatial dimension reduction is applied at the communication receiver, the exact isotropic Gaussian-input rate can be evaluated numerically, revealing a gap to both bounds. A further direction is to characterize the full achievable rate–LMMSE region, beyond the communication-centric point considered here. This includes determining the sensing-optimal performance and its gain over the isotropic Gaussian-signaling LMMSE reported in this work.

ACKNOWLEDGMENT

This work was supported by the ERC under Grant Agreement 101125691.

APPENDIX A
PROOF OF THEOREM 1

We start by proving the expression for the effective communication noise $\sigma_{0,c}^2$ in (24), and then prove the desired upper and lower bounds through comparison of the quantized communication channel (13b) with an auxiliary Gaussian-noise channel of same noise covariance.

A. Effective Communication Noise $\sigma_{0,c}^2$

Under isotropic Gaussian signaling $\mathbf{R}_{\mathsf{X}} = P_0 \mathbf{I}_{N_t}$, and since $\mathbb{E}[\mathsf{HH}^H] = N_t \mathbf{I}_{N_c}$:

$$\mathbb{E}\big[\mathbf{y}_{c,t}\mathbf{y}_{c,t}^H\big] = P_0\,\mathbb{E}[\mathsf{HH}^H] + \sigma_c^2 \mathbf{I}_{N_c} = (N_t P_0 + \sigma_c^2)\mathbf{I}_{N_c}. \quad (38)$$

The semi-unitary constraint (4) implies $\mathbf{R}_{\mathbf{u}_c} = \mathbf{A}_c\,\mathbb{E}[\mathbf{y}_{c,t}\mathbf{y}_{c,t}^H]\,\mathbf{A}_c^H = (N_t P_0 + \sigma_c^2)\mathbf{I}_{\tilde{N}_c}$, so that $\max_i (\mathbf{R}_{\mathbf{u}_c})_{i,i} = N_t P_0 + \sigma_c^2$, irrespective of $\mathbf{A}_c$ and of the realization $\mathbf{H}$. Substituting into (16) recovers (24); in particular, $\sigma_{0,c}^2$ is a constant that depends neither on the combiner nor on the channel.

B. Lower bound

Since the input symbols are i.i.d. across t and the channel is memoryless with effective noise i.i.d. across t, the conditional mutual information single-letterizes,

$$\frac{1}{T}\, I(\mathsf{X}; \mathsf{Z}_c \mid \mathsf{H} = \mathbf{H}) = I(\mathsf{x}_1; \mathsf{z}_{c,1} \mid \mathsf{H} = \mathbf{H}). \quad (39)$$

We therefore drop the time index and write $\mathsf{z}_c = \mathbf{A}_c \mathbf{H} \mathsf{x} + \bar{\mathsf{w}}_c$ with $\mathsf{x} \sim \mathcal{CN}(\mathbf{0}, P_0 \mathbf{I}_{N_t})$.

Notice next that by the worst additivc noise-property of the Gaussian distribution [22], we obtain a lower bound on the mutual information $I(\mathsf{x}; \mathsf{z}_c \mid \mathsf{H} = \mathbf{H})$ by replacing the effective noise $\bar{\mathsf{w}}_c$ with a CSCG vector of the same covariance matrix. $\sigma_{0,c}^2 \mathbf{I}_{\tilde{N}_c}$. For isotropic Gaussian inputs $\mathsf{x} \sim \mathcal{CN}(\mathbf{0}, P_0 \mathbf{I}_{N_t})$, this yields the lower bound

$$I(\mathsf{x}; \mathsf{z}_c \mid \mathsf{H} = \mathbf{H}) \geq \log\det\left(\mathbf{I}_{\tilde{N}_c} + \frac{P_0}{\sigma_{0,c}^2}\,\mathbf{A}_c \mathbf{H}\mathbf{H}^H \mathbf{A}_c^H\right) \quad (40)$$

$$\triangleq g(\mathbf{A}_c). \quad (41)$$

Let now $\mathbf{H}\mathbf{H}^H = \sum_{i=1}^{N_c} \lambda_i(\mathsf{HH}^H)\mathbf{v}_i\mathbf{v}_i^H$ be its eigendecomposition with $\lambda_1(\mathsf{HH}^H) \geq \cdots \geq \lambda_{N_c}(\mathsf{HH}^H)$. Since $\mathbf{A}_c\mathbf{A}_c^H = \mathbf{I}_{\tilde{N}_c}$, the matrix $\mathbf{A}_c\mathbf{H}\mathbf{H}^H\mathbf{A}_c^H$ is a compression of $\mathbf{H}\mathbf{H}^H$, and the Poincaré separation theorem [23, Thm. 4.3.28] yields

$$\lambda_i\big(\mathbf{A}_c\mathbf{H}\mathbf{H}^H\mathbf{A}_c^H\big) \leq \lambda_i(\mathsf{HH}^H), \qquad i = 1, \ldots, \tilde{N}_c, \quad (42)$$

with equality for all i simultaneously when the rows of $\mathbf{A}_c$ are the dominant eigenvectors $\mathbf{v}_1, \ldots, \mathbf{v}_{\tilde{N}_c}$. As $g(\mathbf{A}_c)$ is increasing in each eigenvalue, the maximizer is

$$\mathbf{A}_c^\circ(\mathbf{H}) = \begin{bmatrix}\mathbf{v}_1 & \cdots & \mathbf{v}_{\tilde{N}_c}\end{bmatrix}^H, \quad (43)$$

and

$$\max_{\mathbf{A}_c} g(\mathbf{A}_c) = \sum_{i=1}^{\tilde{N}_c} \log\left(1 + \frac{P_0 \lambda_i(\mathsf{HH}^H)}{\sigma_{0,c}^2}\right). \quad (44)$$

Taking expectation over H yields the desired lower bound in (25).

Fix $\mathbf{H}$ and any semi-unitary $\mathbf{A}_c$. The effective noise $\bar{\mathsf{w}}_c$ has zero mean, covariance $\sigma_{0,c}^2 \mathbf{I}_{\tilde{N}_c}$, and is independent of the Gaussian input. Since Gaussian noise is the worst case additive noise of given noise covariance matrix [22], replacing $\bar{\mathsf{w}}_c$ by a CSCG vector of the same covariance can only decrease the mutual information,

$$I(\mathsf{x}; \mathsf{z}_c \mid \mathsf{H} = \mathbf{H}) \geq g(\mathbf{A}_c). \quad (45)$$

Evaluating (45) at $\mathbf{A}_c^\circ(\mathbf{H})$ and using (44),

$$\max_{\mathbf{A}_c} I(\mathsf{x}; \mathsf{z}_c \mid \mathsf{H} = \mathbf{H}) \geq \sum_{i=1}^{\tilde{N}_c} \log\left(1 + \frac{P_0 \lambda_i(\mathsf{HH}^H)}{\sigma_{0,c}^2}\right). \quad (46)$$

Taking expectation over H yields the desired lower bound $R_{\mathrm{G}} \geq R_{\mathrm{G,L}}$.

C. Upper bound

Fix $\mathbf{H}$ and any semi-unitary $\mathbf{A}_c$. Since the effective noise is independent of the input,

$$I(\mathsf{x};\mathsf{z}_c \mid \mathsf{H}=\mathbf{H}) = h(\mathsf{z}_c \mid \mathsf{H}=\mathbf{H}) - h(\bar{\mathsf{w}}_c). \tag{47}$$

The output covariance is $\mathbf{R}_{\mathsf{z}_c|\mathbf{H}} = P_0\mathbf{A}_c\mathbf{H}\mathbf{H}^H\mathbf{A}_c^H + \sigma_{0,c}^2\mathbf{I}_{\tilde{N}_c}$. Among all complex random vectors with a given covariance, the circularly-symmetric Gaussian maximizes differential entropy [24, Thm. 8.6.5], so

$$\begin{aligned} h(\mathsf{z}_c \mid \mathsf{H}=\mathbf{H}) &\le \log\det\big(\pi e\, \mathbf{R}_{\mathsf{z}_c|\mathbf{H}}\big) \\ &= \tilde{N}_c \log\big(\pi e\, \sigma_{0,c}^2\big) + g(\mathbf{A}_c). \end{aligned} \tag{48}$$

For the noise term, the semi-unitary combiner keeps the receiver noise white, so $\bar{\mathsf{w}}_c$ has i.i.d. entries $\bar{\mathsf{W}}_{c,i}$, each with independent and identically distributed real and imaginary parts; therefore

$$h(\bar{\mathsf{w}}_c) = \tilde{N}_c\, h(\bar{\mathsf{W}}_c) = 2\tilde{N}_c\, h\big(\mathrm{Re}(\bar{\mathsf{W}}_c)\big), \tag{49}$$

where $\mathrm{Re}(\bar{\mathsf{W}}_c)$ is the sum of a $\mathcal{N}(0,\sigma_c^2/2)$ term and an independent $\mathcal{U}[-\Delta_c/2,\Delta_c/2]$ term, with the density (27). Combining (47)–(49), only $g(\mathbf{A}_c)$ depends on the combiner; maximizing over $\mathbf{A}_c$ via (44) and taking expectation over H yields the desired upper bound in (26).

Above proof does not rely on the Gaussian signaling assumption, and thus $R_{\mathrm{G,U}}$ is also an upper bound on capacity.

APPENDIX B
PROOF OF THEOREM 2

We first derive the LMMSE error $\sigma^2_{\mathsf{g}|\mathsf{X}=\mathbf{X}}(\mathbf{A}_s)$ for a fixed realization $\mathsf{X}=\mathbf{X}$ and combiner $\mathbf{A}_s$ in closed form, and then take the expectation over X and minimize over $\mathbf{A}_s$.

A. Conditional LMMSE for a fixed $\mathsf{X}=\mathbf{X}$

Taking the trace of the error covariance (19), substituting $\mathbf{R}_{\mathsf{g}} = \mathbf{R}_B \otimes \mathbf{R}_A$ and $\mathbf{R}_{\bar{\mathsf{w}}_s} = \sigma_{0,s}^2\mathbf{I}_{\tilde{N}_sT}$ from (15), and applying the mixed-product rule $(\mathbf{A}\otimes\mathbf{B})(\mathbf{C}\otimes\mathbf{D}) = \mathbf{AC}\otimes\mathbf{BD}$ so that every factor separates across the two Kronecker blocks, trace cyclicity yields

$$\begin{aligned} &\sigma^2_{\mathsf{g}|\mathsf{X}=\mathbf{X}}(\mathbf{A}_s) \\ &= \frac{1}{N_tN_s}\,\mathrm{Tr}(\mathbf{R}_B\otimes\mathbf{R}_A) \\ &\quad -\frac{1}{N_tN_s}\,\mathrm{Tr}\bigg(\big(\mathbf{X}^T\mathbf{R}_B^2\mathbf{X}^*\otimes\mathbf{A}_s\mathbf{R}_A^2\mathbf{A}_s^H\big) \\ &\qquad\qquad \cdot\Big[\mathbf{X}^T\mathbf{R}_B\mathbf{X}^*\otimes\mathbf{A}_s\mathbf{R}_A\mathbf{A}_s^H + \sigma_{0,s}^2\mathbf{I}_{\tilde{N}_sT}\Big]^{-1}\bigg). \end{aligned} \tag{50}$$

The first trace does not depend on $\mathbf{X}$ and we keep it unchanged. In the following, we first simplify the effective sensing noise variance $\sigma_{0,s}^2$, and then show that the second trace, abbreviated by $f(\mathbf{X})$, reduces to a scalar sum.

From the stacked sensing model, the pre-quantization vector is $\mathsf{u}_s = (\mathsf{X}^T\otimes\mathbf{A}_s)\mathsf{g} + (\mathbf{I}_T\otimes\mathbf{A}_s)\mathsf{w}_s$, so that its covariance matrix is

$$\mathbf{R}_{\mathsf{u}_s} = \mathbb{E}_{\mathsf{X}}\Big[\mathsf{X}^T\mathbf{R}_B\mathsf{X}^*\Big]\otimes\mathbf{A}_s\mathbf{R}_A\mathbf{A}_s^H + \sigma_s^2\mathbf{I}_{\tilde{N}_sT}, \tag{51}$$

and, recalling $\sigma_{0,s}^2 = \sigma_s^2 + \beta\max_i(\mathbf{R}_{\mathsf{u}_s})_{i,i}$ from (16), the effective sensing noise variance is

$$\begin{aligned} \sigma_{0,s}^2 = \beta \max_{i=1,\dots,\tilde{N}_sT}&\Big(\mathbb{E}_{\mathsf{X}}\Big[\mathsf{X}^T\mathbf{R}_B\mathsf{X}^*\Big]\otimes\mathbf{A}_s\mathbf{R}_A\mathbf{A}_s^H\Big)_{i,i} \\ &+\sigma_s^2(1+\beta). \end{aligned} \tag{52}$$

We continue to simplify this expression. For i.i.d. columns $\mathsf{x}_t \sim \mathcal{CN}(\mathbf{0},\mathbf{R}_{\mathsf{X}})$, the (t_1,t_2) entry of $\mathbb{E}_{\mathsf{X}}[\mathsf{X}^T\mathbf{R}_B\mathsf{X}^*]$ is zero for $t_1\neq t_2$ and equals $\mathrm{Tr}(\mathbf{R}_{\mathsf{X}}^*\mathbf{R}_B)$ for $t_1=t_2$, so that $\mathbb{E}_{\mathsf{X}}[\mathsf{X}^T\mathbf{R}_B\mathsf{X}^*] = \mathrm{Tr}(\mathbf{R}_{\mathsf{X}}^*\mathbf{R}_B)\mathbf{I}_T$. Introducing $\bar{\mathbf{A}}_s \triangleq \mathbf{A}_s\mathbf{R}_A^{1/2}$, so that $\mathbf{A}_s\mathbf{R}_A\mathbf{A}_s^H = \bar{\mathbf{A}}_s\bar{\mathbf{A}}_s^H$, (52) becomes

$$\sigma_{0,s}^2 = \beta\ \mathrm{Tr}(\mathbf{R}_{\mathsf{X}}^*\mathbf{R}_B)\max_i\big(\bar{\mathbf{A}}_s\bar{\mathbf{A}}_s^H\big)_{i,i} + \sigma_s^2(1+\beta). \tag{53}$$

Both $f(\mathbf{X})$ and $\mathbf{R}_{\mathsf{u}_s}$ depend on the combiner only through $\bar{\mathbf{A}}_s$, and, as shown later in this appendix, the left singular vectors of $\bar{\mathbf{A}}_s$ affect $f(\mathbf{X})$ through $\max_i(\mathbf{R}_{\mathsf{u}_s})_{i,i}$. We therefore choose them so as to minimize $\max_i(\mathbf{R}_{\mathsf{u}_s})_{i,i}$. Since any Hermitian PSD matrix $\mathbf{M}$ satisfies $\min_{\bar{\mathbf{U}}}\max_i(\bar{\mathbf{U}}\mathbf{M}\bar{\mathbf{U}}^H)_{i,i} = \mathrm{Tr}(\mathbf{M})/\tilde{N}_s$ [25, Cor. 2.4], and since $\mathrm{Tr}(\bar{\mathbf{A}}_s\bar{\mathbf{A}}_s^H) = \sum_i\sigma_i^2$, where $\{\sigma_i\}_{i=1}^{\tilde{N}_s}$ are the singular values of $\bar{\mathbf{A}}_s$, the effective noise variance becomes

$$\sigma_{0,s}^2 = \frac{\beta}{\tilde{N}_s}\,\mathrm{Tr}(\mathbf{R}_{\mathsf{X}}^*\mathbf{R}_B)\sum_{i=1}^{\tilde{N}_s}\sigma_i^2 + \sigma_s^2(1+\beta). \tag{54}$$

The feasible set of the squared singular values $\{\sigma_i^2\}_{i=1}^{\tilde{N}_s}$ follows from $\sum_i\sigma_i^2 = \mathrm{Tr}(\bar{\mathbf{A}}_s\bar{\mathbf{A}}_s^H) = \mathrm{Tr}(\mathbf{A}_s\mathbf{R}_A\mathbf{A}_s^H)$ and the semi-unitary constraint $\mathbf{A}_s\mathbf{A}_s^H = \mathbf{I}_{\tilde{N}_s}$. Denoting by $\lambda_{A,1},\dots,\lambda_{A,N_s}$ the eigenvalues of $\mathbf{R}_A$ in decreasing order, Ky Fan's eigenvalue inequalities [23, Cor. 4.3.39] bound the trace $\mathrm{Tr}(\mathbf{A}_s\mathbf{R}_A\mathbf{A}_s^H)$ between the sums of the $\tilde{N}_s$ smallest and the $\tilde{N}_s$ largest eigenvalues of $\mathbf{R}_A$,

$$\sum_{i=N_s-\tilde{N}_s+1}^{N_s}\lambda_{A,i} \;\le\; \sum_{i=1}^{\tilde{N}_s}\sigma_i^2 \;\le\; \sum_{i=1}^{\tilde{N}_s}\lambda_{A,i}. \tag{55}$$

We next show that, once optimized over $\bar{\mathbf{A}}_s$, the term $f(\mathbf{X})$ reduces to a scalar sum. To this end, for a given realization $\mathbf{X}$, consider the singular value decompositions

$$\mathbf{R}_B^{1/2}\mathbf{X}^* = \mathbf{U}'\mathbf{\Sigma}'\mathbf{V}'^H, \qquad \bar{\mathbf{A}}_s = \mathbf{U}_s\mathbf{\Sigma}_s\mathbf{V}_s^H, \tag{56}$$

with $\mathbf{\Sigma}'\in\mathbb{C}^{N_t\times T}$ and $\mathbf{\Sigma}_s\in\mathbb{C}^{\tilde{N}_s\times N_s}$ rectangular diagonal. Substituting (56) into $f(\mathbf{X})$, using $\mathbf{X}^T\mathbf{R}_B^{1/2} = (\mathbf{R}_B^{1/2}\mathbf{X}^*)^H$ and the trace identity $\mathrm{Tr}(\mathbf{M}_1\mathbf{M}_2) = \mathrm{Tr}(\mathbf{M}_2\mathbf{M}_1)$, the common unitary factor $\mathbf{V}'\otimes\mathbf{U}_s$ cancels and we obtain

$$f(\mathbf{X}) = \mathrm{Tr}\Big[\big(\mathbf{U}'^H\mathbf{R}_B\mathbf{U}'\otimes\mathbf{V}_s^H\mathbf{R}_A\mathbf{V}_s\big)\,\mathbf{D}\Big], \tag{57}$$

with the diagonal matrix $\mathbf{D}\triangleq(\mathbf{\Sigma}'\otimes\mathbf{\Sigma}_s^H)(\mathbf{\Sigma}'^H\mathbf{\Sigma}'\otimes\mathbf{\Sigma}_s\mathbf{\Sigma}_s^H + \sigma_{0,s}^2\mathbf{I})^{-1}(\mathbf{\Sigma}'^H\otimes\mathbf{\Sigma}_s)$. In particular, $f(\mathbf{X})$ does not depend on $\mathbf{U}_s$, which is the left-unitary freedom invoked above.

Let $\lambda_n' \triangleq (\sigma_n')^2$, $n=1,\dots,N_t$, denote the nonzero eigenvalues of $\mathbf{R}_B^{1/2}\mathsf{X}^*\mathsf{X}^T(\mathbf{R}_B^{1/2})^H$, i.e., the nonzero diagonal entries of $\mathbf{\Sigma}'\mathbf{\Sigma}'^H$, and recall that σ_i, $i=1,\dots,\tilde{N}_s$, are the diagonal entries of $\mathbf{\Sigma}_s$. The $\big((n-1)N_s+i\big)$-th diagonal entry of $\mathbf{D}$ is then

$$D_{(n-1)N_s+i} = \frac{\lambda'_n\,\sigma_i^2}{\lambda'_n\,\sigma_i^2+\sigma_{0,s}^2}. \tag{58}$$

By the diagonality of $\mathbf{D}$, only the diagonal entries of $\mathbf{U}'^H\mathbf{R}_B\mathbf{U}'$ and $\mathbf{V}_s^H\mathbf{R}_A\mathbf{V}_s$ contribute to the trace in (57), so that

$$f(\mathbf{X}) = \sum_{n=1}^{N_t}\sum_{i=1}^{\tilde{N}_s} d_{B,n}\,d_{A,i}\,\frac{\lambda'_n\,\sigma_i^2}{\lambda'_n\,\sigma_i^2+\sigma_{0,s}^2}, \tag{59}$$

where $d_{B,n} \triangleq (\mathbf{U}'^H\mathbf{R}_B\mathbf{U}')_{n,n}$ and $d_{A,i} \triangleq (\mathbf{V}_s^H\mathbf{R}_A\mathbf{V}_s)_{i,i}$.

The vector $(d_{A,1},\ldots,d_{A,N_s})$ is majorized by the vector of eigenvalues $(\lambda_{A,1},\ldots,\lambda_{A,N_s})$ of $\mathbf{R}_A$, with equality attained by choosing $\mathbf{V}_s$ to align with the eigenvectors of $\mathbf{R}_A$. Since $f(\mathbf{X})$ is a linear functional of the $d_{A,i}$ with nonnegative coefficients, majorization theory [25, Cor. 2.1] implies that it is maximized by this aligned choice, for which $d_{A,i} = \lambda_{A,i}$, $i = 1,\ldots,\tilde{N}_s$. Equation (59) then becomes

$$f(\mathbf{X}) = \sum_{n=1}^{N_t}\sum_{i=1}^{\tilde{N}_s} d_{B,n}\,\lambda_{A,i}\,\frac{\lambda'_n\,\sigma_i^2}{\lambda'_n\,\sigma_i^2+\sigma_{0,s}^2}. \tag{60}$$

Combining the above, an optimal sensing combiner is $\mathbf{A}_s^\circ = \mathbf{U}_s\mathbf{\Sigma}_s\mathbf{V}_s^H\mathbf{R}_A^{-1/2}$.

B. Expectation over X

In (60), the only quantities that depend on the random waveform X are the eigenvalues $\{\lambda'_n\}$ of $\mathsf{W} = \mathbf{R}_B^{1/2}\mathsf{X}^*\mathsf{X}^T(\mathbf{R}_B^{1/2})^H$ and the diagonal entries $\{d_{B,n}\}$ of $\mathbf{U}'^H\mathbf{R}_B\mathbf{U}'$, where $\mathbf{U}'$ is the eigenvector matrix of W. Since W is a Wishart-type matrix, its eigenvectors are isotropically distributed and statistically independent of its eigenvalues $\{\lambda'_n\}$ [26, Thm. 2.2]. As $d_{B,n}$ is a function of $\mathbf{U}'$ only, this independence lets the expectation of each summand in (60) factor as

$$\mathbb{E}_{\mathsf{X}}\left[d_{B,n}\,\frac{\lambda'_n\,\sigma_i^2}{\lambda'_n\,\sigma_i^2+\sigma_{0,s}^2}\right] = \mathbb{E}_{\mathsf{X}}[d_{B,n}]\;\mathbb{E}_{\mathsf{X}}\left[\frac{\lambda'_n\,\sigma_i^2}{\lambda'_n\,\sigma_i^2+\sigma_{0,s}^2}\right]. \tag{61}$$

By the isotropy of the eigenvectors, each column $\mathbf{u}'_n$ of $\mathbf{U}'$ is uniformly distributed on the unit sphere, hence $\mathbb{E}_{\mathsf{X}}[\mathbf{u}'_n\mathbf{u}'^H_n] = \mathbf{I}_{N_t}/N_t$, and by the cyclicity of the trace,

$$\begin{aligned}\mathbb{E}_{\mathsf{X}}[d_{B,n}] &= \mathbb{E}_{\mathsf{X}}\big[(\mathbf{U}'^H\mathbf{R}_B\mathbf{U}')_{n,n}\big] = \mathbb{E}_{\mathsf{X}}\big[\mathbf{u}'^H_n\mathbf{R}_B\mathbf{u}'_n\big] \\ &= \mathrm{Tr}\big(\mathbf{R}_B\,\mathbb{E}_{\mathsf{X}}[\mathbf{u}'_n\mathbf{u}'^H_n]\big) = \frac{\mathrm{Tr}(\mathbf{R}_B)}{N_t}.\end{aligned} \tag{62}$$

Substituting (61) and (62) into the expectation of (60) gives

$$\mathbb{E}_{\mathsf{X}}[f(\mathsf{X})] = \sum_{n=1}^{N_t}\sum_{i=1}^{\tilde{N}_s}\frac{\mathrm{Tr}(\mathbf{R}_B)}{N_t}\,\lambda_{A,i}\,\mathbb{E}_{\mathsf{X}}\left[\frac{\lambda'_n\,\sigma_i^2}{\lambda'_n\,\sigma_i^2+\sigma_{0,s}^2}\right]. \tag{63}$$

Finally, the conditional distortion (50) equals $\frac{1}{N_tN_s}\mathrm{Tr}(\mathbf{R}_B\otimes\mathbf{R}_A) - \frac{1}{N_tN_s}f(\mathbf{X})$, so minimizing the expected distortion over the sensing combiner amounts to maximizing $\mathbb{E}_{\mathsf{X}}[f(\mathsf{X})]$ over the squared singular values $\{\sigma_i^2\}$ subject to (55). Substituting (63) and (54) into this maximization yields (35), which completes the proof.

References

[1] Y. Zeng, F. Liu, H. Zhang, and Z. Tian, "On the fundamental tradeoff of integrated sensing and communications under Gaussian channels," *IEEE Trans. Commun.*, vol. 71, no. 9, pp. 5726–5740, Sep. 2023.

[2] H. Deng and Y. Zeng, "Fundamental limits of communication-assisted sensing in ISAC systems," *IEEE Trans. Signal Process.*, vol. 70, pp. 6160–6175, 2022.

[3] M. Ahmadipour, M. Kobayashi, M. Wigger, and G. Caire, "An information-theoretic approach to joint sensing and communication," *IEEE Trans. Inf. Theory*, 2022.

[4] M.-C. Chang, S.-Y. Wang, T. Erdoğan, and M. R. Bloch, "Rate and detection-error exponent tradeoff for joint communication and sensing of fixed channel states," *IEEE J. Sel. Areas Inf. Theory*, 2023.

[5] H. Wu and H. Joudeh, "Joint communication and channel discrimination," *Entropy*, vol. 26, no. 12, p. 1089, 2024.

[6] A. Khalili, S. Rini, L. Barletta, E. Erkip, and Y. C. Eldar, "On MIMO channel capacity with output quantization constraints," in *Proc. IEEE ISIT*, Jun. 2018, pp. 1355–1359.

[7] N. Liang and W. Zhang, "MIMO networks with one-bit ADCs: Receiver design and communication strategies," *IEEE Trans. Commun.*, vol. 64, no. 11, pp. 4755–4766, Nov. 2016.

[8] J. Choi, J. Mo, and R. W. H. Jr., "A general framework for MIMO receivers with low-resolution quantization," *IEEE Trans. Signal Process.*, vol. 64, no. 21, pp. 5625–5637, Nov. 2016.

[9] J. Singh, O. Dabeer, and U. Madhow, "On the limits of communication with low-precision analog-to-digital conversion at the receiver," *IEEE Trans. Commun.*, vol. 57, no. 12, pp. 3629–3639, Dec. 2009.

[10] J. Mo and R. W. H. Jr., "Capacity analysis of one-bit quantized MIMO systems with transmitter channel state information," *IEEE Trans. Signal Process.*, vol. 63, no. 20, pp. 5498–5512, Oct. 2015.

[11] H. Atrsaei, M. Sarkiss, and M. Wigger, "Channel capacity under the subtractive dithered quantization model," 2026, unpublished.

[12] W. Weichselberger, M. Herdin, H. Özcelik, and E. Bonek, "A stochastic MIMO channel model with joint correlation of both link ends," *IEEE Trans. Wireless Commun.*, vol. 5, no. 1, pp. 90–100, Jan. 2006.

[13] F. Liu, C. Masouros, A. Alexiou, H. V. Poor, and L. Hanzo, "Integrated sensing and communications: Toward dual-functional wireless networks for 6G and beyond," *IEEE J. Sel. Areas Commun.*, vol. 40, no. 6, pp. 1728–1767, Jun. 2022.

[14] H. Ruan and F. Liu, "Task-based quantizer design for sensing with random signals," in *Proc. IEEE ISIT*, 2024, pp. 1806–1811.

[15] N. Shlezinger, Y. C. Eldar, and M. R. D. Rodrigues, "Asymptotic task-based quantization with application to massive MIMO," *IEEE Trans. Signal Process.*, vol. 67, no. 15, pp. 3995–4012, Aug. 2019.

[16] ——, "Hardware-limited task-based quantization," *IEEE Trans. Signal Process.*, vol. 67, no. 20, pp. 5223–5238, Oct. 2019.

[17] L. Schuchman, "Dither signals and their effect on quantization noise," *IEEE Trans. Commun. Technol.*, vol. 12, no. 4, pp. 162–165, Dec. 1964.

[18] R. M. Gray and T. G. Stockham, "Dithered quantizers," *IEEE Trans. Inf. Theory*, vol. 39, no. 3, pp. 805–812, May 1993.

[19] S. M. Kay, *Fundamentals of Statistical Signal Processing: Estimation Theory*. Prentice Hall, 1993.

[20] E. Björnson, J. Hoydis, and L. Sanguinetti, "Massive MIMO networks: Spectral, energy, and hardware efficiency," *Found. Trends Signal Process.*, vol. 11, no. 3–4, pp. 154–655, 2017.

[21] W. C. Jakes and D. C. Cox, *Microwave Mobile Communications*. Wiley–IEEE Press, 1994.

[22] S. Diggavi and T. Cover, "The worst additive noise under a covariance constraint," *IEEE Trans. Inf. Theory*, vol. 47, no. 7, pp. 3072–3081, 2001.

[23] R. A. Horn and C. R. Johnson, *Matrix Analysis*, 2nd ed. Cambridge University Press, 2012.

[24] T. M. Cover and J. A. Thomas, *Elements of Information Theory*, 2nd ed. Wiley-Interscience, 2006.

[25] D. P. Palomar and Y. Jiang, *MIMO Transceiver Design via Majorization Theory*. Now Publishers, 2007.

[26] R. Couillet and M. Debbah, *Random Matrix Methods for Wireless Communications*. Cambridge University Press, 2011.